



CHORUS

This is the accepted manuscript made available via CHORUS. The article has been published as:

Self-Organization, Structures, and Anomalous Transport in Turbulent Partially Magnetized Plasmas with Crossed Electric and Magnetic Fields

Oleksandr Koshkarov, Andrei Smolyakov, Yevgeny Raitses, and Igor Kaganovich

Phys. Rev. Lett. **122**, 185001 — Published 7 May 2019

DOI: [10.1103/PhysRevLett.122.185001](https://doi.org/10.1103/PhysRevLett.122.185001)

Self-organization, structures, and anomalous transport in turbulent $\mathbf{E} \times \mathbf{B}$ partially magnetized plasmas

Oleksandr Koshkarov* and Andrei Smolyakov

*Department of Physics and Engineering Physics,
University of Saskatchewan, Saskatoon SK S7N 5E2, Canada*

Yevgeny Raitses and Igor Kaganovich

Plasma Physics Laboratory, Princeton University, Princeton, New Jersey 08543, USA

(Dated: April 15, 2019)

Self-organization and anomalous transport in gradient-drift driven turbulence in partially magnetized plasmas with crossed electric and magnetic fields is demonstrated in two-dimensional fluid simulations. The development of large scale structures and flows is shown to occur as a result of the inverse energy cascade from short wavelength instabilities. The turbulence shows complex interaction of small scale modes with large scale zonal flows modes, vortices, and streamers resulting in strongly intermittent anomalous transport which significantly exceed the classical collisional values. The turbulence driven secondary instabilities and large scale structures are shown to dominate the anomalous electron current. Such anomalous transport and structures are consistent with a number of experimental observations in laboratory plasmas.

Partially magnetized plasmas with crossed electric and magnetic fields is common occurrence in many laboratory plasma devices [1–4] and space conditions [5]. Due to large spatial and temporal scale separation, ($\rho_e \ll L \ll \rho_i$ where ρ_e, ρ_i are electron and ion Larmor radii respectively, L is a system size) the nature of plasma instabilities and nonlinear physics in such plasmas is different from situations in which both components (electron and ions) are magnetized. Many incarnations of such plasmas show development of various instabilities [1, 6, 7] leading to turbulence, structures, and anomalous electron current. Despite wide occurrence, nonlinear physics of such plasmas, in particular, the nature of the instabilities, turbulence saturation, and associated anomalous transport is not well understood.

The picture of basic eigen-modes and instabilities in partially magnetized $\mathbf{E} \times \mathbf{B}$ plasmas is somewhat different from the standard case of fully magnetized plasmas. The standard electron drift waves [8] are absent in plasmas with unmagnetized ions, but there exists the specific density gradient eigen-mode with the frequency $\omega = \omega_{ci} k_y L_n$ [9], where $L_n = (n_0^{-1} \partial_x n_0)^{-1}$ is the density gradient length scale, k_y is the wavevector in the direction of the density gradient and perpendicular to the magnetic field $\mathbf{B}_0 = B_0 \hat{\mathbf{z}}$, $\omega_{ci} = eB_0/m_i c$ is the ion cyclotron frequency. This quasineutral mode exists for purely transverse propagation with wavevector parallel to the magnetic field $k_z = 0$ (contrary to the standard drift waves in fully magnetized plasma). For smaller scales and higher frequencies, the inertial response of electrons becomes important resulting in the lower-hybrid modes $\omega = \omega_{LH} \equiv \sqrt{\omega_{ce} \omega_{ci}}$, where ω_{ce} is electron cyclotron

frequency. The model can be extended into the third dimension with appropriate boundary conditions along the magnetic field [10]. The local linear theory however predicts the strongest instabilities for modes with $k_z = 0$, which are therefore subject of our studies here.

The transverse electron current due the electron $\mathbf{E} \times \mathbf{B}$ drift is a major driver of instabilities in partially magnetized crossed-fields plasmas. In the long wavelength regime, when the electron inertia can be neglected, the reactive instability occurs for $\mathbf{E}_0 \cdot \nabla n_0 > 0$, which is usually called the collisionless Simon-Hoh instability [11–14]. For shorter wavelength, when the electron inertia is involved, the lower-hybrid mode can be destabilized by plasma gradients as well as collisions [15–17].

In this paper we study the turbulent regimes of gradient-drift and lower-hybrid modes using the nonlinear reduced fluid model [16]. In this model, two-dimensional (in the x, y plane perpendicular to the magnetic field) nonlinear equation for electrons is

$$(\partial_t + u_0 \partial_y) \eta = n_0 v_* \partial_y \frac{e\phi}{T_e} - \nu(\eta - n) + \omega_{ce} \rho_e^2 \left\{ \frac{e\phi}{T_e}, \eta \right\}, \quad (1)$$

Here $\eta = n + \rho_e^2 (n_0 \nabla^2 e\phi / T_e - \nabla^2 n)$ is the generalized vorticity, n, n_0 are respectively the perturbed and equilibrium electron density, ϕ is a perturbed electrostatic potential, u_0 is the equilibrium electron $\mathbf{E} \times \mathbf{B}$ drift, ν is an electron-neutral collision frequency, $\{f, g\} = \partial_x f \partial_y g - \partial_y f \partial_x g$ is a Poisson bracket.

The velocity of unmagnetized ions is represented as $\mathbf{V}_i = v_0 \hat{\mathbf{x}} - \nabla \chi$, where v_0 is the equilibrium ion flow, and χ is the "potential" function describing the perturbed ion velocity. Then, the ion continuity and momentum balance equations are

$$(\partial_t + v_0 \partial_x) n = (n_0 + n) \nabla^2 \chi + \nabla n \cdot \nabla \chi, \quad (2)$$

$$(\partial_t + v_0 \partial_x) \chi = c_s^2 \frac{e\phi}{T_e} + \frac{1}{2} (\nabla \chi)^2. \quad (3)$$

* Current address: T-5 Applied Mathematics and Plasma Physics Group, Los Alamos National Laboratory, Los Alamos, New Mexico, USA

The equilibrium electric field, equilibrium ion velocity, and the density gradient are along the \hat{x} axis, and the equilibrium electron $\mathbf{E} \times \mathbf{B}$ drift is in the \hat{y} direction. Therefore, Cartesian coordinates (x, y, z) correspond to the axial, azimuthal, and radial directions of the cylindrical geometry of the Hall thrusters and magnetrons, $(z, \phi, r) \rightarrow (x, y, z)$, and for cylindrical Penning discharge configuration with the axial magnetic field, $(r, \phi, z) \rightarrow (x, y, z)$, respectively.

For further studies, we use the following dimensionless parameters $L_n = 48.8\rho_e$, $u_0 = 241.8c_s$, $v_0 = 3.72c_s$, $\nu = 0.28\omega_{LH}$, $\sqrt{m_i/m_e} = 427$, which roughly correspond to Hall thruster parameters [18], e.g. such as $E = 2 \times 10^4$ V/m, $B = 200$ G, $T_e = 17.7$ eV, $v_0 = 15$ km/s, $u_0 = 10^6$ m/s, $L_n = 2.45$ cm, $\nu = 2.3$ MHz.

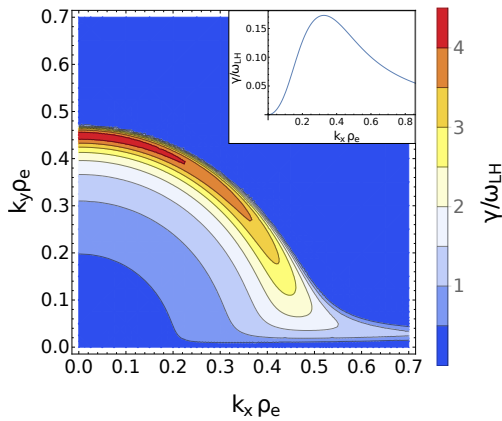


FIG. 1: Linear growth rate. Insert shows $k_y = 0$ slice.

From Eq. (1)-(3), the linear dispersion equation [16] for the long wavelength Simon-Hoh instability and [13, 14] and short wavelength lower hybrid modes [17, 19] is:

$$\frac{c_s^2 k^2}{(\omega - v_0 k_x)^2} = \frac{v_* k_y + \rho_e^2 k^2 (\omega - u_0 k_y + i\nu)}{\omega - u_0 k_y + \rho_e^2 k^2 (\omega - u_0 k_y + i\nu)}. \quad (4)$$

For our parameters, the growth rate is shown in Fig. 1 where the most unstable modes have $\gamma = \text{Im}(\omega) \sim 4\omega_{LH}$. It is important to note that the dispersion relation (4) also reveals a pure axial linear instability with $k_x \neq 0$, $k_y = 0$ of the resistive nature Refs. [20–22]. For our parameters, the growth rate of the axial instability is of order $\gamma = 0.15\omega_{LH}$, and it is shown in the one dimensional slice $k_y = 0$ on the insert of Fig. 1. As it is discussed below, despite the relatively slow growth rate, the resistive axial instability plays an important role in 2D nonlinear dynamics and turbulent transport.

Nonlinear Eqs. (1)-(3) are solved with double-periodic boundary conditions and for constant density gradient (as well as for $L_n = \infty$), and constant v_0 , u_0 , using BOUT++ framework employing FFT along y and finite difference with WENO reconstruction along x together with CVODE time integration solver [23]. Temporal and spatial resolutions were varied to achieve convergence and to resolve linear spectrum predicted by the dispersion

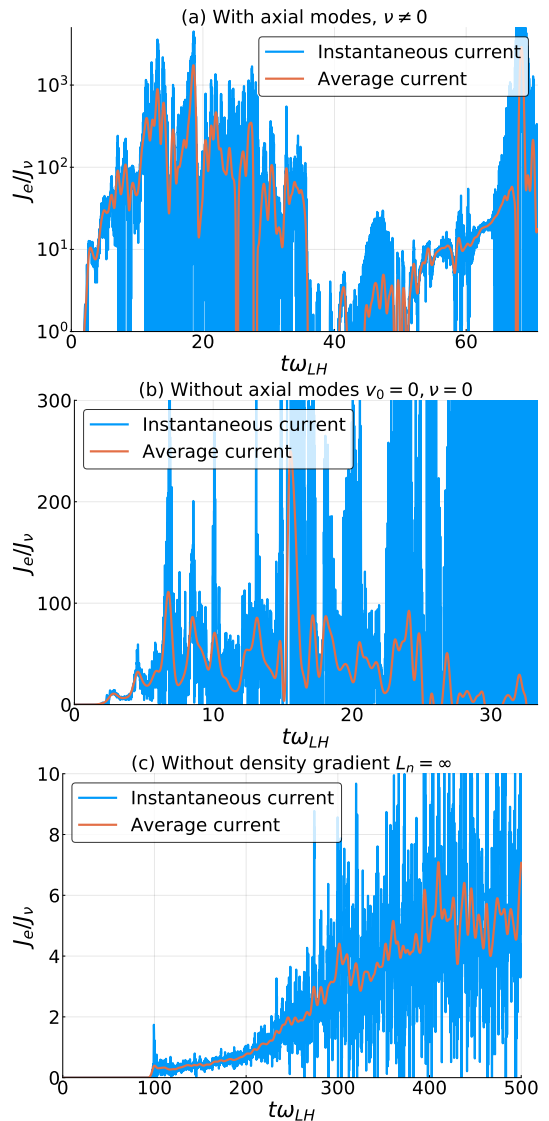


FIG. 2: Anomalous axial electron current.

equation (4) with error less than 10%. The hyperviscosity of fourth order ($\partial_t \sim \nabla^4$) was added to simulations to avoid numerical instability, but its amplitude was chosen sufficiently small in order not to change significantly linear or nonlinear stages of simulations. All simulations (unless stated otherwise) were performed until the nonlinear saturation of the wave energy is reached [16, 24]. The linear growth benchmarking against analytical theory were reported in Ref. [16, 24].

One of the main results of our study is the first-principle demonstration of significant turbulent (anomalous) electron current driven by gradient-drift turbulence of azimuthal modes in $\mathbf{E} \times \mathbf{B}$ plasmas shown in Fig 2. It shows axial current evolution for different parameters: (a) — for full system; (b) — in the absence of ion flow and collisions ($v_0 = \nu = 0$); (c) — in the absence of equilibrium density gradient ($L_n = \infty$). As is evident from Fig. 2a, the turbulent elec-

tron current is orders of magnitude larger than the classical (collisional) axial current. The anomalous current J_e due to turbulent $\mathbf{E} \times \mathbf{B}$ drift was evaluated as $j_e = -ecn\partial_y\phi/B$, $J_e = \int j_e dx dy / (L_x L_y)$, and shown in Fig. 2 [25] in units of classical collisional current J_ν corresponding to classical conductivity $\sigma_\nu = e^2 n_0 \nu / m_e \omega_{ce}^2$. It can be recast in units of the effective Hall parameter, $\Omega = (\omega_{LH}/\nu)(m_i/m_e)^{1/2}(J_e/J_\nu)^{-1}$, thus $\Omega \simeq 15$ for $J_e \sim 100J_\nu$, which is generally consistent with experimental values in Hall thrusters and results of PIC modeling [26].

To investigate the nature and the role of large scale structures, we have performed simulations turning off the resistivity and ion velocity, by setting $\nu = 0$ and $v_0 = 0$, thus removing the linear resistive axial instability, which leads to a noticeably smaller anomalous current (shown in Fig 2b).

The gradient-drift instability in nonlinear stage produces large scale azimuthally elongated (along $\hat{\mathbf{y}}$ axis) shear zonal flows, $k_x \gg k_y$, which subsequently form large scale vortices via mechanism similar to Kelvin-Helmholtz instability as shown in Figs. 3a and 3b. Those structures occur on the length scale significantly larger than the scale of the most unstable linear modes in Fig. 1 which indicates the inverse cascade predicted analytically for partially magnetized plasmas in Ref. [27]. The vortices are quasi-stable, i.e. they exist for period of time comparable to the largest growth rate ($t \sim \omega_{LH}^{-1}$), then collapsing back into shear flows and reappearing again at larger and larger length scale (up to the size of the simulation box).

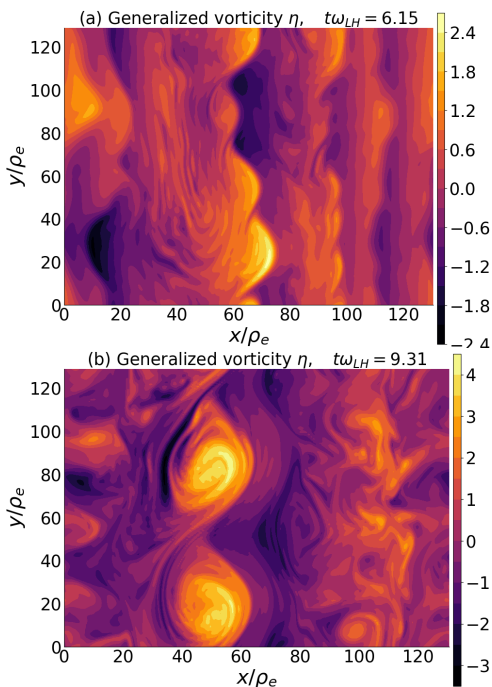


FIG. 3: Shear flows and vortices in simulation with $v_0 = 0$ and $\nu = 0$.

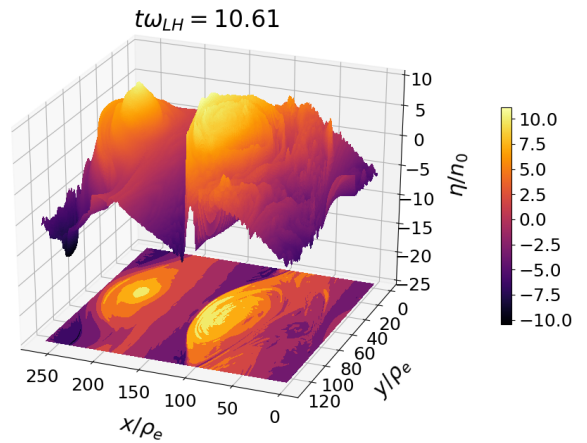


FIG. 4: Coexisting small scale fluctuations, large scale vortices and axial modes in simulation with $\nu = 0$.

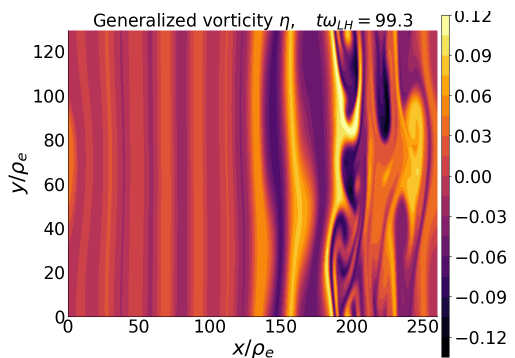


FIG. 5: Generation of azimuthal modes by axial modes in simulation without density gradient $L_n = \infty$.

Nonlinear formation of zonal flow type axial structures due to the inverse cascade is further enhanced by the linear and nonlinear instabilities of the axial modes, which, in presence of the ion flow $v_0 \neq 0$, produced by a finite electron-neutral collision frequency ν [22] or as a secondary instability of the anomalous electron current produced by small scale gradient-drift fluctuations.

The axial modes in absence of the linear axial electron current ($J_\nu \sim \sigma_\nu \sim \nu = 0$) are shown in Fig. 4. In this case, the nonlinear axial current (created by small scale turbulence) becomes unstable via the mechanism similar to the linear axial resistive instability with $\nu \neq 0$. The exponential growth of the axial modes driven by the anomalous current was demonstrated earlier [24]. As a result, large amplitude axial mode is present together with azimuthal drift waves and vortices. Note the high amplitude axial variations in generalized vorticity visible in 3D rendering of Fig. 4. In simulations involving axial modes, the axial system size L_x was increased to allow larger wavelengths of the nonlinearly generated axial modes. As it was shown in Ref. [24] the axial modes are saturated by nonlinear terms in ion equations (2) and (3).

The turbulent electron current in the presence of ax-

ial modes is larger compared to the case when the linear axial modes were turned off, compare Fig. 2a with Fig. 2b. It is important to note that axial modes itself do not produce any axial electron transport and can affect it only via the excitation and enhancement of the azimuthal modes. To confirm the generation of the azimuthal modes (and thus the axial anomalous current) by the axial modes we have performed the simulations where underlying gradient-drift modes are removed ($L_n = \infty$) and axial mode linear instability is initially the only mode driven by collisions. Note that the remaining instability of resistive azimuthal modes [17] is much weaker than the axial instability so that in the linear phase ($t < 90\omega_{LH}^{-1}$), only axial modes are present in the system. Our simulation shows the slow excitation and nonlinear saturation of the axial mode, consistent with results of Ref. [22]. When the axial mode grows to large amplitude, the axial density variations (induced by axial mode) become sufficiently large for the excitation of secondary azimuthal gradient-drift waves for $t \sim 100\omega_{LH}^{-1}$, as shown in Fig. 5 with anomalous current shown in Fig. 2c.

Thus, our nonlinear simulations have revealed the following phenomena and stages in the nonlinear evolution of the system (1)-(3): (i) the most unstable small scale gradient-drift waves are excited and grow exponentially in time; the nonlinear turbulent state is formed dominated by nonlinear effects from the Poisson bracket term in (1); the large scale shear flows form due to the inverse cascade with subsequent development of vortices (similar to Kelvin-Helmholtz instability); the turbulence significantly enhances the axial electron conductivity; (ii) the anomalous electron current triggers the axial instability and axial modes grow; (iii) axial modes saturate into a high amplitude axial structures [22]. The saturation mechanism for axial modes is nonlinearities in the ion equations and therefore their saturation amplitude are much larger than that of gradient-drift waves. As a result, the axial modes significantly change the density and electric field profiles, affecting the underlying gradient-drift instabilities.

The generalized vorticity profile for full equations is shown in Fig. 6a. We also report the existence of quasi-stable axial streamers existing up to $t\omega_{LH} \sim 5$ in our simulations. Streamers are axially elongated and azimuthally localized structures providing large contribution to the axial anomalous current. The large streamer is shown in Fig. 6b. We should note that streamers also appear in the absence of axial modes ($v_0 = 0$).

In this letter, we investigated the nonlinear gradient-drift and lower-hybrid instabilities in partially magnetized plasmas with crossed electric and magnetic fields. These modes are expected to play a central role in formation of long wavelength structures and transport in various devices employing $\mathbf{E} \times \mathbf{B}$ configurations for electric propulsion [1, 3, 28], material processing [2, 6, 29], and cylindrical Penning type devices [4, 30, 31]. The large scale structures (shear zonal flows and vortices) are produced via the inverse cascade of the energy flow

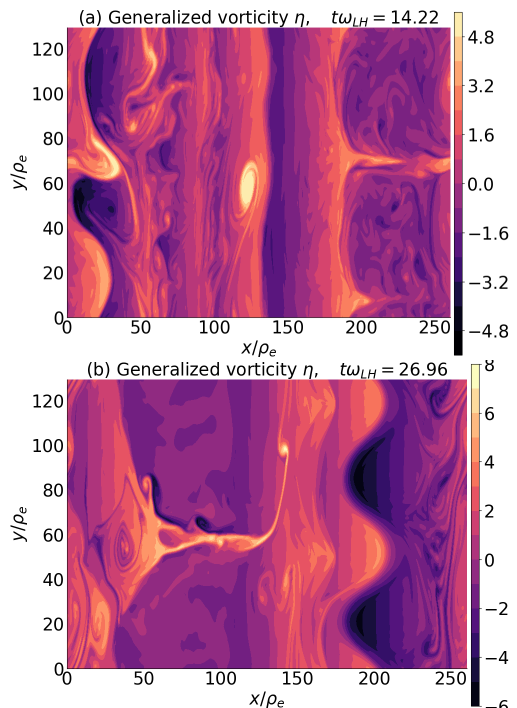


FIG. 6: Shear flows, vortices, axial modes, and streamers in simulation of full system.

from short wavelength modes. The turbulence self-organization in our simulations is further enhanced by coupling to the axial modes produced by linear and nonlinear mechanisms. This coupling is twofold: (i) the anomalous current produced by nonlinear interaction of azimuthal gradient-drift modes results in a strong drive of the axial instability, thus enhancing its growth; (ii) the axial modes modify the density and electric profiles, providing feedback on turbulent azimuthal modes. The ensuing turbulence demonstrate the complex interactions of large scale shear flows, vortices, and streamers that produce anomalous electron current orders of magnitude higher than the collisional current. This suggests that turbulent transport observed in $\mathbf{E} \times \mathbf{B}$ experiments [32, 33] and kinetic simulations [26, 34] can be explained as a result of turbulence driven by gradient-drift modes. A notable feature of the anomalous current in presence of large scale structures is its intermittent and blobby nature [32], as it is also shown in our simulations, Fig. 2. Such anomalous current cannot credibly be parameterized by the enhanced transport coefficients, such as mobility, but rather requires avalanche like approaches as in self-organized-criticality models with transport event at different scales [35].

We have confirmed [24] that fluctuation energy is well saturated in our simulations, the anomalous transport, however, as shown in Figs. 2a and 2b is not necessarily saturated at long time scales. We consider this as another manifestation of the intermittency. In part, it could be attributed to inadequate saturation mechanisms of large

scale structures in our model. The model assumptions of constant gradients should be revised at later times, when coherent structure sizes becomes comparable to the simulation box size. Therefore, the long time evolution of anomalous current will be affected by the device geometry and self-consistent modification of the mean profiles (gradients) which are not accounted for in considered model. It should be noted that the simplified slab geometry used in this work does not describe properly the finite and curvature effects. Such effects are expected to

be important for large scale structures of the order of the box size, however the general conclusions regarding the inverse cascade and anomalous transport are expected to remain valid.

This work was supported in part by NSERC Canada, the Air Force Office of Scientific Research under awards FA9550-18-1-0132 and FA9550-15-1-0226, and computational resources from Compute Canada/WestGrid. The authors would like to express their gratitude to Prof M. Cappelli for insightful discussions and suggestions in the course of this work.

-
- [1] J. P. Boeuf and B. Chaudhury, *Physical Review Letters* **111**, 155005 (2013).
- [2] S. Tsikata and T. Minea, *Physical Review Letters* **114**, 185001 (2015).
- [3] B. A. Jorns, I. G. Mikellides, and D. M. Goebel, *Physical Review E* **90**, 063106 (2014).
- [4] G. R. Tynan *et al.*, *Plasma Physics and Controlled Fusion* **48**, S51 (2006).
- [5] M. E. Koepke, *Reviews of Geophysics* **46**, 3001 (2008).
- [6] T. Ito, C. V. Young, and M. A. Cappelli, *Applied Physics Letters* **106**, 254104 (2015).
- [7] X. L. Zhang, R. S. Fletcher, and S. L. Rolston, *Physical Review Letters* **101**, 195002 (2008).
- [8] F. F. Chen, *Introduction to plasma physics and controlled fusion* (Springer, 2016).
- [9] A. M. Fridman, *Soviet Phys Dokl* **9**, 75 (1964).
- [10] V. Morin and A. I. Smolyakov, *Physics of Plasmas* **25** (2018), 10.1063/1.5044649.
- [11] A. Simon, *Physics of Fluids* **6**, 382 (1963).
- [12] F. C. Hoh, *Physics of Fluids* **6**, 1184 (1963).
- [13] Y. Sakawa *et al.*, *Physical Review Letters* **69**, 85 (1992).
- [14] Y. Sakawa *et al.*, *Physics of Fluids B-Plasma Physics* **5**, 1681 (1993).
- [15] Y. V. Esipchuk and G. N. Tilinin, *Sov. Phys. Tech. Phys.* **21**, 417 (1976).
- [16] A. I. Smolyakov *et al.*, *Plasma Physics and Controlled Fusion* **59**, 13 (2017).
- [17] A. A. Litvak and N. J. Fisch, *Physics of Plasmas* **8**, 648 (2001).
- [18] A. I. Morozov and V. V. Savelyev, *Reviews of Plasma Physics* **21**, 203 (2000).
- [19] R. C. Davidson and N. T. Gladd, *Physics of Fluids* **18**, 1327 (1975).
- [20] S. Chable and F. Rogier, *Physics of Plasmas* **12**, 033504 (2005).
- [21] E. Fernandez *et al.*, *Physics of Plasmas* **15**, 012102 (2008).
- [22] O. Koshkarov *et al.*, *Physics of Plasmas* **25**, 011604 (2018).
- [23] B. D. Dudson *et al.*, *Computer Physics Communications* **180**, 1467 (2009).
- [24] O. Koshkarov, Ph.D. thesis, University of Saskatchewan (2018).
- [25] The average current in Fig. 2 is computed with 3 point unweighted sliding-average filter applied subsequently 500 times (the current data is saved every $0.1\omega_{LH}^{-1}$).
- [26] I. Katz, V. H. Chaplin, and A. L. Ortega, *Physics of Plasmas* **25**, 123504 (2018).
- [27] V. P. Lakhin *et al.*, *Physics of Plasmas* **23**, 7 (2016).
- [28] A. Lazurenko, V. Vial, M. Prioul, and A. Bouchoule, *Physics of Plasmas* **12** (2005), 013501 10.1063/1.1818698.
- [29] A. Anders, P. Ni, and A. Rauch, *Journal of Applied Physics* **111**, 053304 (2012).
- [30] A. M. DuBois *et al.*, *Physics of Plasmas* **21**, 062117 (2014).
- [31] T. R. Desjardins and M. Gilmore, *Physics of Plasmas* **23**, 055710 (2016).
- [32] J. B. Parker, Y. Raitses, and N. J. Fisch, *Applied Physics Letters* **97**, 091501 (2010).
- [33] A. N. Smirnov, Y. Raitses, and N. J. Fisch, *IEEE Transactions on Plasma Science* **34**, 132 (2006).
- [34] A. T. Powis *et al.*, *Physics of Plasmas* **25**, 072110 (2018).
- [35] P. A. Politzer, *Phys. Rev. Lett.* **84**, 1192 (2000).